arXiv:1301.5879v2 [cond-mat.mtrl-sci] 28 Feb 2013

Evolutionary Method for Predicting Surface Reconstructions with Variable Stoichiometry: Implementation in the USPEX Code and Application to GaN $(10\bar{1}1)$ Surface with Oxygen Adatoms

Qiang Zhu,[1,*] Li Li,[2] Artem R. Oganov,[1,2,3] and Philip B. Allen[2]

[1]*Department of Geosciences, Stony Brook University, Stony Brook, New York 11794, USA*
[2]*Department of Physics and Astronomy, Stony Brook University, Stony Brook, New York 11794, USA*
[3]*Geology Department, Moscow State University, Moscow 119992, Russia*

We present a specially designed evolutionary algorithm for the prediction of surface reconstructions. This new technique allows one to automatically explore all the low-energy configurations with variable surface atoms and variable surface unit cells through the whole chemical potential range. Using this method to study the reconstructions of the GaN $(10\bar{1}1)$ surface with and without absorbate oxygen, we find a non-intuitive reconstruction based on N_3-trimers. The method can be generally applied to binary and multi-component systems.

INTRODUCTION

At crystalline surfaces, especially in semiconductors, atoms rearrange to form reconstructed configurations, which are different from those in the bulk crystals. Reconstructions play a key role in surface properties, such as epitaxial crystal growth, catalysis, etc. Determining the reconstruction of semiconductor surfaces is a long-standing problem. Despite progress in experimental techniques, it is still hard to obtain the atomic-scale details. Diffraction and microscopy can yield the periodicity and symmetry [1, 2]. However, the sampling space is astronomically large, and solutions may defy intuition, even for monoatomic systems: consider Si(111) 7×7 [3–5]. For binary and more complex cases, a variable stoichiometry at the surface adds a huge extra dimension.

From the computational perspective, the main difficulty lies in that the number of candidate structures is extremely large. It is not possible to enumerate all the reasonable reconstruction models just from chemical intuition. There have been a few efforts towards automatic prediction of the most stable configuration for either a given stoichiometry [6–8], or a variable composition at constant chemical potential [9]. With these structural models available, the thermodynamical phase diagram can thus been constructed [10]. However, unbiased predicting reconstructions with variable stoichiometry in the whole chemical potential range has not been attempted to our knowledge. In this letter, we propose a new method which allows automatic exploration of all low-energy configurations, with variable surface atoms and variable reconstruction cells through the whole chemical potential range. We apply this method to GaN $(10\bar{1}1)$ surfaces with and without added oxygen.

THEORETICAL BACKGROUND

Surface Energy and Chemical Potential

Relative stability among candidate surfaces is determined by the formation energy $E_{\text{formation}}$

$$E_{\text{formation}} = E_{\text{tot}} - E_{\text{ref}} - \sum_i n_i \mu_i, \tag{1}$$

where E_{tot} and E_{ref} is the total energy of the surface under consideration and of the reference cleaved surface, n_i and μ_i are the number and chemical potential for each species, respectively. The chemical potential is the energy to add or remove one atom from the system, assuming there is a reservoir for each species to equilibrate with. The chemical potentials must satisfy constraints. For example in a simple binary AB compound, the chemical potential of A (or B) is bounded above by the chemical potential of elemental A (or B),

$$\begin{aligned} \mu_{\text{A}} &\leq E_{\text{A}} \\ \mu_{\text{B}} &\leq E_{\text{B}}. \end{aligned} \tag{2}$$

The A and B atoms are in equilibrium with the substrate,

$$\mu_{\text{A}} + \mu_{\text{B}} = E_{\text{AB}}. \tag{3}$$

These conditions lead to the range of the A component chemical potential to be

$$E_{\text{AB}} - E_{\text{B}} \leq \mu_{\text{A}} \leq E_{\text{A}}. \tag{4}$$

Therefore, Eq. (1) can be rewritten as only μ_{A} dependent

$$E_{\text{formation}} = E_{\text{tot}} - E_{\text{ref}} - n_{\text{B}} E_{\text{AB}} - \mu_{\text{A}}(n_{\text{A}} - n_{\text{B}}). \tag{5}$$

The surface phase diagram shows which reconstruction is favored under a specific environment, i.e., temperature and chemical potential or partial pressure of each component. Each of these environmental conditions represents an independent dimension in the phase diagram.

Evolutionary algorithm

We employ an evolutionary algorithm (EA) to explore the surface structures. The algorithm is implemented in the USPEX package, which has been successfully applied to various bulk materials [11–14]. We use a representation in which the system has three parts: vacuum, surface and substrate. Vacuum and substrate regions are pre-specified, while surface region is optimized by the EA. The number of surface atoms varies up to the maximum for a given thickness of surface. To allow automatic exploration of reconstructions with different surface unit cells, the cell size is also variable.

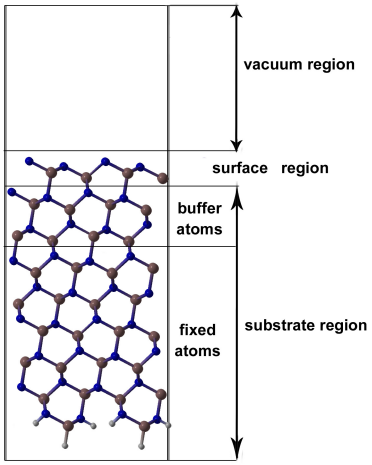

FIG. 1. Surface representation used in the evolutionary algorithm.

Our algorithm is constructed in the following way. It first generates random structures with only the surface region being varied. These initial structures are then relaxed, and ranked by its fitness, based on the energy. Structures with better fitness are more likely to be selected as parents to generate new child structures. We considered three ways to produce offspring.

(i) Heredity: Two structures are chosen from the previous generation. They are randomly sliced at the same position in the surface unit cell. Then pieces from both parent structures are combined to generate the offspring.

(ii) Mutation: One structure is chosen as parent. Similar to the implementation of softmutation in bulk crystals [15], the surface atoms are mutated according to the softest surface vibrational modes based on the bond-hardness model [16, 17]. If the structure cannot be softmutated anymore, we switch to the coordinate mutation [15], which is to randomly mutate the surface atoms from a zero-mean Gaussian distribution.

(iii) Transmutation: One structure is chosen as parent. Some atoms are transmuted to another type of chemical identity.

The offsprings, together with a few best structures from the previous generation, comprise the next generation. This process is repeated until no new ground-state structures are produced for sufficiently many generations. As a test, we applied the EA search to study the known 2×1 reconstructions of diamond (100) and (111) surfaces. We tried 2 and 6 carbon atoms on a 2×1 surface cell. During the search, each structure was first relaxed with the Brenner potential [18] as implemented in the GULP code [19], and then more accurate energy evaluation was performed at *ab initio* level with PBE functional [20] as implemented in the VASP code [21]. Fig. 2 shows the best structures found in the search. The ground state of diamond (100) surface contains characteristic C dimers (Fig. 2a), while the most stable configuration of diamond (111) surface indicates a rather complex reconstruction. Different from the bulk structure, the surface atoms form the 5+7 ring topology from the side view (Fig. 2b, it is noteworthy that such peculliar 5+7 ring topology can even form three dimensional structure via cold compression of graphite [22, 23]). Our results are in excellent agreement with those shown in the previous literature [24]. We also performed the predictions for 4 and 12 carbon atoms on a 2×2 cell, but only with the Brenner potential. Although Brenner potential gives wrong energy ranking, the true ground states were also found as a low-energy configurations in the search. With this encouragement, we proceed to the case of more than one specie and variable stoichiometry.

Fitness function

Our fitness function needs to indicate the relative stability of the structures with various surface stoichiometry and reconstruction cell sizes. We illustrate this in Fig. 3. First, for two given surface configurations (I and II) which have different numbers of atoms on the same substrate cell, their relative energy difference depends on the chemical potential $\mu_{\rm A}$ according to Eq.(5). As shown in Fig. 3a, surfaces I and II should coexist at $\mu_{\rm A} = \mu_{\rm eq}$. Therefore, the stability regime for the two surfaces can be fully established. Surface I is stable when $\mu_{\rm min} \leq \mu_{\rm A} \leq \mu_{\rm eq}$, while surface II is stable when $\mu_{\rm eq} \leq \mu_{\rm A} \leq \mu_{\rm max}$. For any other unstable configuration like surface III, the fitness can be viewed as the minimum energy difference comparing with the stable configuration, at all possible chemical potentials. The minimum condition is reached when $\mu_{\rm A} = \mu_{\rm eq}$. For practical implementation it is useful to express this algebraically. We define $E_0 = E_{\rm tot} - E_{\rm ref} - n_{\rm B}E_{\rm AB}$ as the $\mu_{\rm A}$-independent term in Eq.(5). This approach was introduced by Qian *et al* [25], and is widely used [26]. Versions (a) and (b) of Fig. 3 contain equivalent information. The stable structures appearing in the phase diagram form a convex hull. The slope of each section of the convex hull is either the boundary chemical potential or the equilibrium chemical potential where stable structures can coexist. We then choose the fitness of a surface structure to be its distance to the convex hull. The EA search then aims to optimize the convex hull, similar to our previously proposed approach of variable composition prediction for bulk crystals [12, 27]. When different sizes of surface cell ($m \times n$) occur, the scale factor $N_{\rm cell} = m \times n$ should be taken into account and energies have to be normalized.

RESULTS AND DISCUSSIONS

We studied the reconstructions on the semipolar GaN $(10\bar{1}1)$ surfaces in the presence of oxygen. As a global optimization method, an EA search requires hundreds or thousands of individual structural relaxations. In our calculation, relaxations were done using DFT within the generalized gradient approximation (GGA) [20] using the all-electron projector augmented wave (PAW) [28] method as implemented in

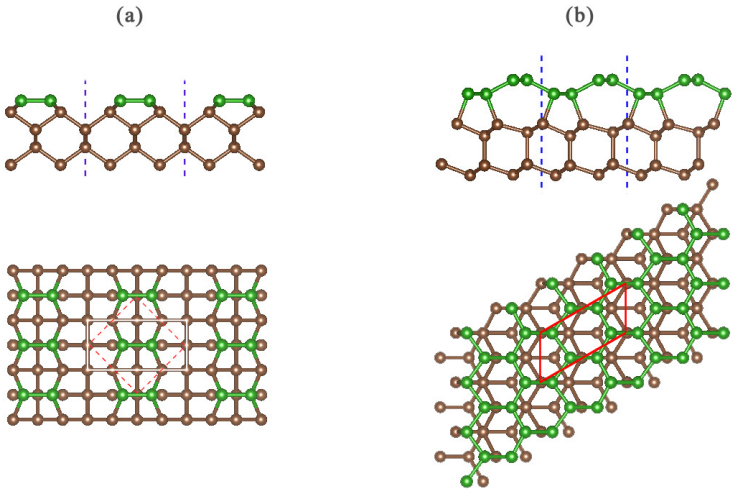

FIG. 2. Schematic image of (a) diamond (100) 2×1 reconstruction (red dashed line: face of conventional cube; white rectangle: 2×1 surface unit cell); (b) diamond (111) 2×1 reconstruction (red rectangle: 2×1 surface unit cell).

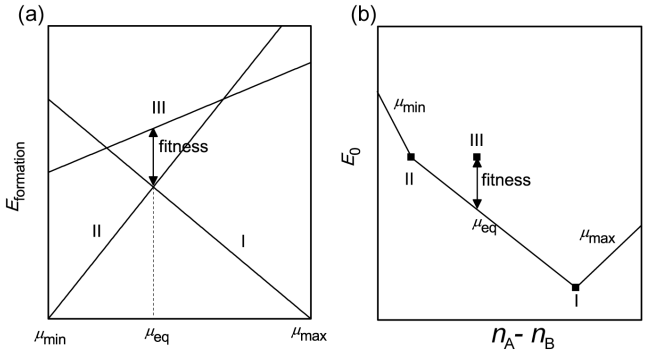

FIG. 3. Illustration of the fitness function used in the evolutionary algorithm. a). Phase diagram as a function of μ_A. b). Phase diagram as a function of $(n_A - n_B)$. The vertices of the convex hull are the stable structures appearing in the phase diagram. The slope of each section of the convex hull is either the boundary chemical potential or the equilibrium chemical potential where stable structures can coexist.

the VASP code [21]. We used the kinetic energy cutoff of 550 eV for the plane-wave basis set and Brillouin zone sampling resolution of $2\pi \times 0.08$ Å^{-1}, which showed excellent convergence of the energy differences, stress tensors and structural parameters. Dipole corrections to the electrostatic potentials are also included to partly cancel the interactions between the slab and its images [29, 30]. The bottom surface is passivated by fractional hydrogens [31]. The passivated surface is semiconducting, with no surface states in the fundamental band gap of GaN. For trial calculations, the slab contains 5 layers of GaN, with the top 2 layers being relaxed. To obtain accurate surface energies, we use a slab containing 10 layers with the top 5 layers relaxed. Our tests suggest that the surface energy is converged to better than 0.05 eV per surface cell. Our surface calculations are restricted to a 2×2 or smaller surface cell.

Fig. 4a gives the convex hull diagram from our EA search, and the five corresponding stable structures. Compared to the cleaved surface (Fig. 4c), structure S1 has two Ga adlayers. Structure S2 has one Ga adlayer. Structure S3 has the top N and half of the second N removed. Structure S4 has only the top N removed. Structure S5 has an additional N at the bridging position of the two top N atoms. The first 4 structures have been found by Akiyama *et al* [32]. Structure S5, was not reported before and is not intuitively obvious. This demonstrates the power of the automated searching by the evolutionary algorithm. An analogous Se-trimer feature has been predicted to be stable on ZnSe (100) reconstructions at Se-rich conditions [33]. Compared to the cleaved surface, the stable structures can be constructed through either vacancies or adatoms. No more complicated reconstructions have been found. For the Ga-rich conditions, there are many intermediate structures between structure S1 and S2, lying very close to the convex hull (see Fig. 4). This can be explained by the weak directionality of the Ga-Ga bonds. These structures may appear under finite temperatures. For the N-rich conditions, however, most structures are much higher above the convex hull, due to the strong covalent bonding nature of N-N interactions.

The features possessed by the stable configurations are: i) Ga layers; ii) N vacancies; iii) N trimers. Another common feature is N_2-dimers [33] (these donot lie on the convex hull, but indeed frequently appear as energetically competitive in our EA search).

The electron counting (EC) rule [34–36] emerges from the study of semiconductor surfaces. This rule, although not exact, is very useful in comparing surface energies, estimating surface charges and guessing surface reconstructions. It states that the surface structures with filled dangling bonds on the electronegative elements and empty dangling bonds on the electropositive elements are the lowest in energy. The sur-

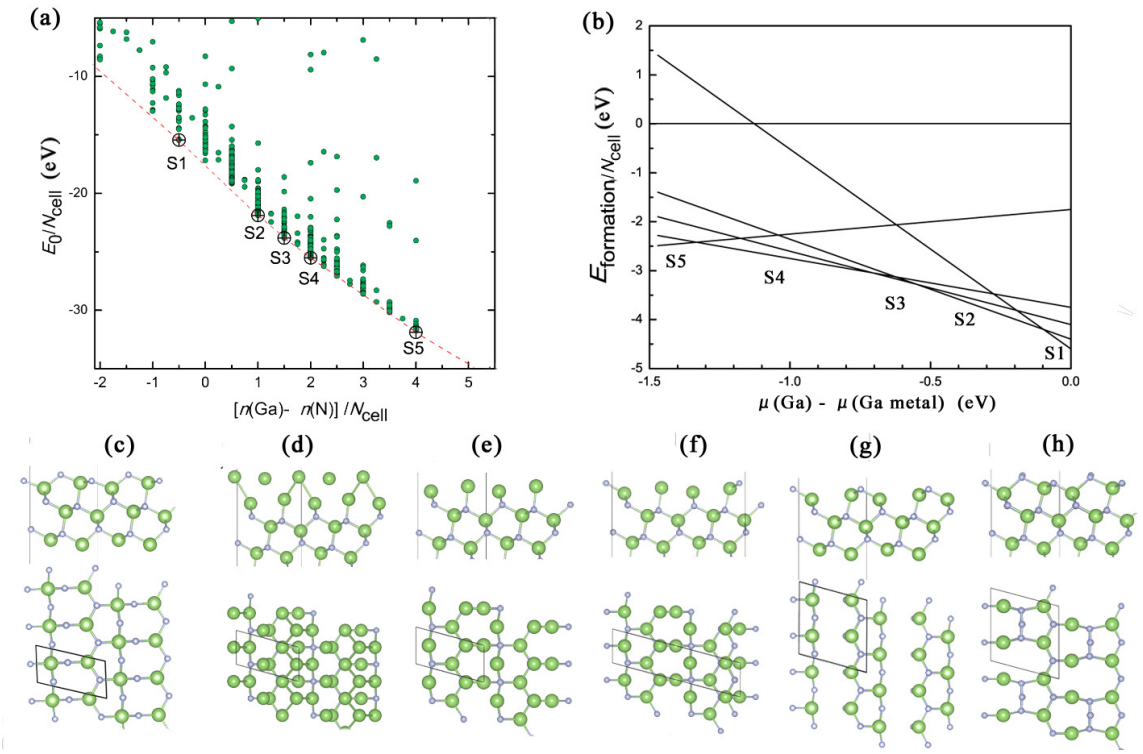

FIG. 4. (a) Energies of GaN$(10\bar{1}1)$ surface reconstructions explored by the evolutionary algorithm; (b) the corresponding zero temperature phase stability diagram up to 2 × 2 supercell reconstructions. Side view and top view of (c) the cleaved GaN$(10\bar{1}1)$ surface and its lower-energy reconstructions found by the EA search; (d) S1 configuration: (1×1) Ga-bilayer; (e) S2 configuration: (1×1) Ga-monolayer; (f) S3 configuration: (2×1)-1.5 N vacancy; (g) S4 configuration: (2×1)-1 N vacancy; (h) S5 configuration: (2×1) N-trimer. Large spheres, gallium; small spheres, nitrogen.

face then is likely to be semiconducting. Surfaces not satisfying this rule will be metallic and higher in energy. None of the stable reconstructions found here satisfy the electron counting rule. Large reconstructions may satisfy the EC rule. Indeed, Lee and Kim [37] demonstrated that low-energy semiconducting surfaces can be achieved by large reconstructions, complying with EC rule by the modulation of N dimer and dimer-vacancy. Due to the limitation of computational power, we are only able to predict the reconstructions up to 2 × 2 surface cells. But our results provide a starting point for predicting large reconstructions.

Let us now employ the same method to search for reconstructions of GaN$(10\bar{1}1)$ surfaces with added oxygen. The formation energy can be defined as

$$E_{\text{formation}} = E_0 - \mu(\text{Ga})[n(\text{Ga}) - n(\text{N})] - \mu(\text{O})n(\text{O}). \quad (6)$$

The oxygen chemical potential μ(O) is a new variable. It has no lower bound, but would possibly reach the upper bound by the constraints based on the possible O_2, N_xO_y molecular gas and Ga_2O_3 solid:

$$\begin{aligned} \mu(\text{O}) &\leq \frac{1}{2}E(\text{O}_2), \\ 2\mu(\text{Ga}) + 3\mu(\text{O}) &\leq E(\text{Ga}_2\text{O}_3), \\ x\mu(\text{Ga}) + y\mu(\text{O}) &\leq E(\text{N}_x\text{O}_y). \end{aligned} \quad (7)$$

Therefore, the convex hull has two dimensions in n(O) and $[n(\text{Ga}) - n(\text{N})]$. Fig. 5a shows the two-dimensional phase diagram in space of μ(O) and $[\mu(\text{N}) - \mu(\text{Ga})]$ transformed from the convex hull found in our EA search. The two new major reconstructions are structure S6 and S7. Compared to the cleaved surface, structure S6 has half of the top N removed, half of the top N and all of the second N replaced by O. Structure S7 has the top two N replaced by O. Similar reconstructions for the $(10\bar{1}1)$ surface have been reported [38]. These reconstructions are favored because of the strong Ga-O bond and the electron counting rule. For example, the simple cleaved surface has 3 nitrogen dangling bonds per surface cell. Because each N dangling bond needs 3/4 electron to become filled, the surface needs 9/4 electrons per surface unit cell to satisfy the electron counting rule. For structure S7, substituting 2 N with 2 O introduces 2 extra electrons. Therefore, it only needs 1/4 electron to satisfy the electron counting rule.

CONCLUSIONS

In summary, we present a specially designed method to automatically explore low energy surface reconstructions with variable surface atoms and reconstruction cells. The power of

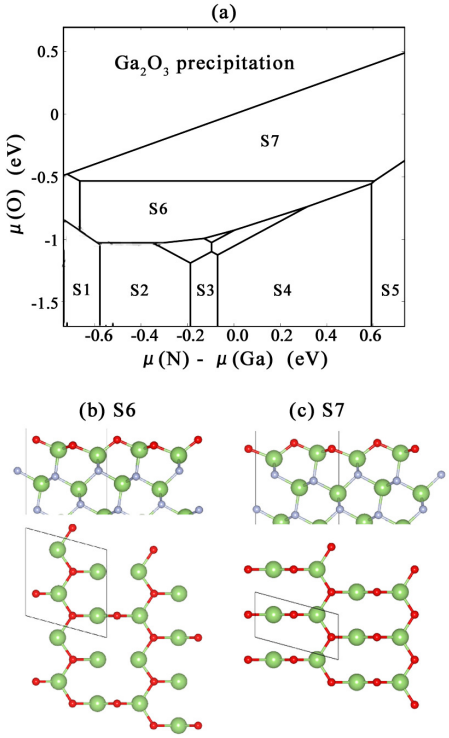

FIG. 5. (a) Phase diagram of the GaN$(10\bar{1}1)$ surface with oxygen present up to 2×2 supercell reconstructions. Important reconstructions are labeled from S1 to S7. Structures S1 to S5 are shown in Fig. 4. Side view and top view of structures S6 and S7 are shown in (b) and (c). Large balls, gallium; small gray balls, nitrogen; small red balls, oxygen.

this approach is illustrated by the identification of N_3 trimeric reconstruction of GaN$(10\bar{1}1)$ surfaces. This method can be generally applied to other binary and even multi-component systems.

PBA and LL thank the SWaSSiT collaboration, and in particular, M. V. Fernandez-Serra, M. S. Hybertsen, and J. T. Muckerman, for help. Calculations were performed at the supercomputer of Center for Functional Nanomaterials, Brookhaven National Laboratory, which is supported by the U.S. Department of Energy, Office of Basic Energy Sciences, under contract No. DE-AC02-98CH10086, and at joint Supercomputer Center of the Russian Academy of Sciences and on Skif supercomputer (Moscow State University). This work is funded by DARPA (grants W31P4Q1210008 and W31P4Q1310005), National Science Foundation (No. EAR-1114313) and DOE (No. DE-FG02-08ER46550).

* qiang.zhu@stonybrook.edu

[1] Q.-K. Xue, Q. Z. Xue, R. Z. Bakhtizin, Y. Hasegawa, I. S. T. Tsong, T. Sakurai, and T. Ohno, Phys. Rev. Lett. **82**, 3074 (1999).
[2] A. Reinert, C. Payne, L. Wang, J. Ciston, Y. Zhu, and P. Khalifah, Preprint, submitted to Inorg. Chem. (2013), this paper identifies the $(10\bar{1}1)$ surface in powders of GaN/ZnO alloy, but says little about the structure of that surface.
[3] R. E. Schlier and H. E. Farnsworth, J. Chem. Phys. **30**, 917 (1959).
[4] K. Takayanagi, Y. Tanishiro, S. Takahashi, and M. Takahashi, Surf. Sci. **164**, 367 (1985).
[5] K. D. Brommer, M. Needels, B. Larson, and J. D. Joannopoulos, Phys. Rev. Lett. **68**, 1355 (1992).
[6] F. Chuang, C. Ciobanu, V. Shenoy, C. Wang, and K. Ho, Surf. Sci. **573**, L375 (2004).
[7] R. M. Briggs and C. V. Ciobanu, Phys. Rev. B **75**, 195415 (2007).
[8] D. Mei, L. Xu, and G. Henkelman, J. Phys. Chem. C **113**, 4522 (2009), http://pubs.acs.org/doi/pdf/10.1021/jp808211q.
[9] M. Sierka, T. K. Todorova, J. Sauer, S. Kaya, D. Stacchiola, J. Weissenrieder, S. Shaikhutdinov, and H.-J. Freund, J. Chem. Phys. **126**, 234710 (2007).
[10] K. Reuter and M. Scheffler, Phys. Rev. Lett. **90**, 046103 (2003).
[11] A. R. Oganov and C. G. Glass, J. Chem. Phys. **124**, 244704 (2006).
[12] A. R. Oganov, A. O. Lyakhov, and M. Valle, Acc. Chem. Res. **44**, 227 (2011).
[13] Q. Zhu, A. R. Oganov, C. W. Glass, and H. T. Stokes, Acta Cryst. B **68**, 215 (2012).
[14] A. O. Lyakhov, A. R. Oganov, H. T. Stokes, and Q. Zhu, Comp. Phys. Comm. **184**, 1172 (2013).
[15] A. O. Lyakhov, A. R. Oganov, and M. Valle, Comp. Phys. Comm. **181**, 1623 (2010).
[16] K. Li, X. Wang, F. Zhang, and D. Xue, Phys. Rev. Lett. **100**, 235504 (2008).
[17] A. O. Lyakhov and A. R. Oganov, Phys. Rev. B **84**, 092103 (2011).
[18] D. W. Brenner, Phys. Rev. B **42**, 9458 (1990).
[19] J. Gale and A. Rohl, Mol. Simul. **29**, 291 (2003).
[20] J. P. Perdew, K. Burke, and M. Ernzerhof, Phys. Rev. Lett. **77**, 3865 (1996).
[21] G. Kresse and J. Furthmüller, Phys. Rev. B **54**, 11169 (1996).
[22] S. E. Boulfelfel, A. R. Oganov, and S. Leoni, Sci. Rep. **2**, 471 (2012).
[23] Y. Wang, J. E. Panzik, B. Kiefer, and K. K. Lee, Sci. Rep. **2**, 520 (2012).
[24] J. Ristein, Surf. Sci. **600**, 3677 (2006).
[25] G.-X. Qian, R. M. Martin, and D. J. Chadi, Phys. Rev. B **38**, 7649 (1988).
[26] J. C. Thomas, N. A. Modine, J. M. Millunchick, and A. Van der Ven, Phys. Rev. B **82**, 165434 (2010).
[27] W. Zhang *et al.*, arXiv preprint arXiv:1211.3644 (2012).
[28] P. E. Blochl, Phys. Rev. B **50**, 17953 (1994).
[29] J. Neugebauer and M. Scheffler, Phys. Rev. B **46**, 16067 (1992).
[30] G. Makov and M. C. Payne, Phys. Rev. B **51**, 4014 (1995).
[31] K. Shiraishi, J. Phys. Soc. Jpn. **59**, 3455 (1990).
[32] T. Akiyama, D. Ammi, K. Nakamura, and T. Ito, Phys. Rev. B **81**, 245317 (2010).
[33] A. Garcia and J. E. Northrup, Appl. Phys. Lett. **65**, 708 (1994).
[34] M. D. Pashley, Phys. Rev. B **40**, 10481 (1989).
[35] S. B. Zhang and S.-H. Wei, Phys. Rev. Lett. **92**, 086102 (2004).
[36] L. Zhang, E. G. Wang, Q. K. Xue, S. B. Zhang, and Z. Zhang, Phys. Rev. Lett. **97**, 126103 (2006).
[37] W.-J. Lee and Y.-S. Kim, Phys. Rev. B **84**, 115318 (2011).
[38] J. E. Northrup, Phys. Rev. B **73**, 115304 (2006).